HHS Public Access

Author manuscript

J Comp Neurol. Author manuscript; available in PMC 2017 June 15.

Published in final edited form as:

J Comp Neurol. 2016 June 15; 524(9): 1859–1875. doi:10.1002/cne.23926.

The Anatomical Basis for Modulatory Convergence in the Antennal Lobe of *Manduca sexta*

Kristyn M. Lizbinski[1], **Jackie D. Metheny**[1,2], **Samual P. Bradley**[1], **Aditya Kesari**[1], and **Andrew M. Dacks**[1]

Thomas E. Finger

University of Colorado School of Medicine: Sensory Systems, Neurobiology of Non-mammalian Vertebrates

[1]Department of Biology, West Virginia University, Morgantown, WV, 26505, United States of America

[2]Center for Cardiovascular and Pulmonary Research and The Heart Center at Nationwide Children's Hospital, Columbus, Ohio 43205

Abstract

The release of neuromodulators by widely projecting neurons often allows sensory systems to alter how they process information based on the physiological state of an animal. Neuromodulators alter network function by changing the biophysical properties of individual neurons and the synaptic efficacy with which individual neurons communicate. However, most, if not all, sensory networks receive multiple neuromodulatory inputs and the mechanisms by which sensory networks integrate multiple modulatory inputs are not well understood. Here, we characterized the relative glomerular distribution of two extrinsic neuromodulators associated with distinct physiological states, serotonin (5-HT) and dopamine (DA), in the antennal lobe (AL) of the moth *Manduca sexta*. Using immunocytochemistry and mass dye fills, we characterized the innervation patterns of both 5-HT and tyrosine hydroxylase immunoreactive processes (TH-ir) relative to each other, olfactory receptor neurons (ORNs), projection neurons (PNs) and several subsets of local interneurons (LNs). 5-HT-ir had nearly complete overlap with PNs and LN, yet no overlap with ORNs, suggesting that 5-HT may modulate PNs and LNs directly but not ORNs. TH-ir overlapped with PNs, LNs and ORNs suggesting that dopamine has the potential to modulate all three cell types. Furthermore, the branching density of each neuromodulator differed with 5-HT exhibiting denser arborizations and TH-ir processes being more sparse. Our results suggest that 5-HT and DA extrinsic neurons target partially overlapping glomerular regions, yet DA extends further into the region occupied by ORNs.

Graphical Abstract

"Using immunocytochemistry and mass dye fills to highlight the processes of specific antennal lobe neuron populations, the authors show that widely projecting serotonergic and dopaminergic

Corresponding author: Andrew M. Dacks, PO Box 6057 Morgantown, WV 26506, tel: 304-293-3205 fax: 304-293-6363, andrew.dacks@mail.wvu.edu.

Conflict of interest statement: The authors declare no conflicting interests

neurons innervate overlapping functional zones within olfactory glomeruli. The relative distribution of these projections demonstrate potential for multiple extrinsic modulatory inputs to converge upon a single network.”.

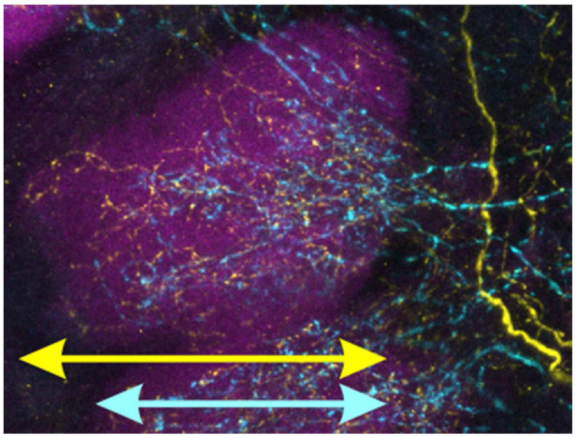

Keywords

neuromodulation; dopamine; serotonin; olfaction; insect

Introduction

The nervous system adjusts the response properties of individual neural networks based on the current physiological state in order to optimize network function (Nusbaum and Marder, 1989; Fontanini and Katz, 2006; Hurley and Hall, 2011; Komuniecki et al., 2014; Su and Wang, 2014). This is often accomplished by widely projecting neurons that respond to changes in the physiological state and release neuromodulators that alter the synaptic efficacy or biophysical properties of individual neurons (Kupfermann, 1979; Kaczmarek and Levitan, 1987; Katz, 1999) with single neuromodulators potentially having wide-ranging and diverse effects on a network. Although a network is constrained by its anatomical layout, modulation of synaptic and cellular mechanisms influences its functional connectivity (Getting, 1989). Thus, the process of neuromodulation expands the dynamic range of a network by adjusting the response properties and interactions of a constant set of neurons. Every neural network is influenced by a dynamic cocktail of multiple neuromodulators (Brezina, 2010; Bargmann, 2012; Marder, 2012; Nusbaum and Blitz, 2012) and single neurons integrate their effects. Overall, many factors, including receptor type, second messenger system, and connectivity allow neuromodulation to provide a remarkable degree of control over network parameters. While the convergence of multiple neuromodulators within a network has been studied extensively in motor systems, the consequences of this convergence in sensory systems has not received as much attention.

To understand the potential impact of modulatory convergence within a sensory system, we sought to first characterize the relative anatomical distribution of multiple neuromodulators within a single sensory system. The physiological effects of serotonin (5-HT) and dopamine (DA) have been well-characterized individually in the olfactory system of *Manduca sexta*

thus making this model system well-positioned to study their combined effects. The first synaptic neuropil of the insect olfactory system, the antennal lobe (AL), is a network comprised of three primary neuron types. Odor-responsive olfactory receptor neurons (ORNs) on the antennae project centrally to the AL where they terminate in ~63 sub-structures called glomeruli (Rospars and Hildebrand, 2000; Huetteroth and Schachtner, 2005). Within each glomerulus, ORNs provide input to projection neurons (PNs) and the transfer of information from ORNs to PNs is refined by local interneurons (LNs) that interconnect each glomerulus. The glomeruli surround a "coarse neuropil" containing the thicker processes of LNs and PNs in which there are little, if any, sites of synaptic interaction (reviewed in Ache and Young, 2005). The orientation of glomeruli is considered with respect to the coarse neuropil, with the proximal half of the glomerulus facing the coarse neuropil and the distal half of the glomerulus facing away from the coarse neuropil. PNs and LNs innervate glomeruli from the proximal end whereas ORNs innervate glomeruli from the distal end.

In addition to these three primary neuron types, a variety of extrinsic neurons project to the AL including two sets of widely projecting neurons releasing 5-HT (Kent et al., 1987) and DA (Dacks et al., 2012). Both modulators enhance neuronal excitability and odor evoked responses in isolation (Kloppenburg and Hildebrand, 1995; Mercer et al., 1995; Mercer et al., 1996; Kloppenburg et al., 1999; Kloppenburg and Heinbockel, 2000; Dacks et al., 2008; Dacks et al., 2012), but their anatomical convergence within individual glomeruli is unknown. The goal of this study was to determine the relative glomerular distribution of 5-HT and DA with relation to the primary neuron types in the AL of *Manduca sexta*. We found that the relative distribution of the processes of both 5-HT and DA neurons suggests that both modulators are more likely to have convergent effects upon LNs and PNs, while DA neurons are more likely to influence ORNs.

Materials and Methods

Animals

Manduca sexta (hereafter referred to as *Manduca*) was raised at West Virginia University on a 16:8 reverse light:dark cycle in the laboratory of Dr. Kevin Daly as previously described (Bell and Joachim, 1976; Daly et al., 2013). Equal numbers of males and females were used and a minimum of 6 moths were used for each protocol.

Immunocytochemistry

Table 1 provides the complete list of antibodies used in this study. Brains were dissected in physiological saline (Christensen and Hildebrand, 1987), fixed in 4% paraformaldehyde overnight at 4°C, run through a dehydrating ethanol series and then embedded in 5% agarose to be sectioned at 100um using a Leica VT 1000S vibratome with the exception of tissue labeled for GABA (75 um) and BRP, *Manduca* tyrosine hydroxylase MsTH and 5-HT triple label (250 um). Sections were washed in PBS with 1% Triton X-100 (PBST), blocked in PBST and 2% IgG free BSA (Jackson Immunoresearch; Cat#001-000-161) and then incubated in blocking solution with 5mM sodium azide and primary antibody. Incubation period and temperature, as well as dilution, were primary antibody specific (see *Antibody*

Characterization section and Table 1). Sections were washed with PBST, blocked as above and fluorescent secondary antibodies against the primary antibody host species were applied overnight at a dilution of 1:1000 at room temperature with the exception of the anti-BRP antibody which was incubated at 4°C. The fluorescent secondary antibodies used (all from Life Technologies) were donkey α-rabbit Alexa 488 (Cat# A-21206), donkey α-mouse Alexa 546 (Cat# A10036) and donkey α-goat Alexa 633 (Cat# A-21082). Sections were then briefly washed with PBS (pH 6.9), PBST, and a series of ascending glycerol washes and then mounted on slides with Vectashield (Vector Laboratories; Cat#H-1000). For peptide pre-adsorptions, all custom lyophilized peptides were synthesized by GenScript. To obtain the *Manduca* specific peptide sequences, we performed a forward protein BLAST analysis of the *Drosophila* pre-propeptide sequence for TKK and MIP in the *Manduca* genome (Agricultural Pest Genomics Resource Database: www.agripestbase.org). Using the top matches from the *Manduca* genome, we then reverse blasted the sequence from the *Manduca* genome into the *Drosophila* genome to ensure that our result returned the lowest E values, indicating that our sequence shared close homology to the *Drosophila* peptide sequence that we used as a reference. The peptide sequences used for pre-adsorption controls had high sequence identity with *Drosophila* TKK_1 (RAPMGFMGVR in *Manduca*) and MIP_{VI} (AWSALHGAWA in *Manduca*).

Dye fills

Antennal nerve fills were performed as previously described (Dacks et al., 2010) using Dextran, Texas Red®, 3000 MW, Neutral (LifeTechnologies, Cat# D-3329). Brains were dissected after 24 hours for subsequent immunocytochemistry. For mushroom body dye fills, moths were waxed into tubes with their heads tilted dorsally, a window cut in the head capsule to expose the mushroom bodies and Dextran, Texas Red was injected into each mushroom body using a pulled glass capillary tube. The cuticle was placed back over the window, the window sealed with petroleum jelly and brains were dissected out for subsequent immunocytochemistry 48-72 hours later to allow diffusion of dye. Moths were fed high concentration sugar water before the dye injection and on each subsequent day to increase survival rates.

Antibody Characterization

Bruchpilot (BRP)—The BRP antiserum (nc-82: Developmental Studies Hybridoma Bank) was raised in mouse against the *Drosophila melanogaster* protein “Bruchpilot” (Hofbauer, 1991) which is a homologue of the presynaptic active zone protein ELKS/CAST and is required for functional synapses in the nervous system of *Drosophila* (Wagh et al., 2006). This antibody is used in many insect species to delineate brain neuropil allowing visualization of brain regions and their individual compartments (Ito et al., 2014). We used the BRP antibody to delineate glomerular boundaries within the AL of *Manduca* and although the purpose of using this antibody was not to study the distribution of the *Manduca* homologue of ELKS/CAST, we performed a Western blot to verify that the antibody labeled a single protein at the predicted height for the *Manduca* homologue of ELKS/CAST. Using the *Manduca* genome (Agricultural Pest Genomics Resource Database: www.agripestbase.org) we performed a forward protein BLAST analysis of the *Drosophila* Bruchpilot amino acid sequence. The top match from the *Manduca* genome had an e-value

of 0.0 and a predicted molecular weight of 234.63kDa. We then reverse blasted the sequence from the *Manduca* genome into the *Drosophila* genome and the first 7 matches were Bruchpilot isoforms, all of which had e-values of 0.0. The next highest match from the *Drosophila* genome had an e-value of 0.71, indicating that the sequence pulled from the *Manduca* genome had a very high sequence homology to *Drosophila* Bruchpilot and almost no homology to other proteins. To ensure that there were not two potential predicted protein sequences from the *Manduca* genome with high sequence homology to *Drosophila* Bruchpilot, we took the amino acid sequence from the *Manduca* genome with the second highest e-value for the *Drosophila* Bruchpilot (e-value = 7e-38) and ran a BLAST analysis of that amino acid sequence in the *Drosophila* genome. The BLAST analysis resulted in an e-value of 0.0 for the *Drosophila* protein Stretchin-MLCK (Champagne et al., 2000), indicating that the *Manduca* protein with the next closest sequence similarity to *Drosophila* Bruchpilot was not a Bruchpilot homologue.

We performed a western blot of *Manduca* brain tissue using the BRP antibody (Fig. 1A). Before dissections, insects were kept on ice for 5 to 60 minutes. Immediately after dissection, brains were placed in Bolt ™ LDS Sample Buffer (Life Technologies; Cat#B0007) with protease inhibitor cocktail (Research Products International; Cat# P50900) and DNase I (Invitrogen;Cat#18068-015) and kept on ice. Tissue was homogenized using a pestle. Bolt ™ Sample Reducing Agent (Life Technologies; Cat# B0009) was added if appropriate. Samples were heated in a water bath for 10 minutes at 95°C. We used the Novex® Bolt™ Gel Electrophoresis System (Life Technologies) with Tris-Glycine SDS Running Buffer at 165V for 2.5 hours and Bolt™ 4-12% Bis-Tris Plus Precast Gels (BG04120BOX) to resolve proteins. We used the iBlot® Gel Transfer Device (Life Technologies; Cat#IB1001) program P0 (20 V for 1 min, 23 V for 4 min, 25 V for 2 min) to transfer proteins to nitrocellulose membranes (nitrocellulose iBlot® Transfer Stacks, Life Technologies; Cat# IB3010-01). We followed the WesternBreeze® Chromogenic Western Blot Immunodetection Kit (Cat#WB7103, anti-mouse) protocol to detect proteins. The BRP antibody was diluted 1:100. Images of membranes were taken with FluorChem Q using Alpha View Analysis Software. Western blot analysis resulted in a single band at the predicted height of ~230 kDa (Fig. 1A). For immunocytochemistry, sectioned tissue was incubated for 172 hours at a dilution of 1:50.

5-HT—The 5-HT antibody (Immunostar, cat# 20079) was raised in goat against serotonin coupled to bovine serum albumin with paraformaldehyde. Pre-adsorption of the antiserum by incubating with 1mg/mL BSA and 10:1 5-HT-BSA conjugate (Immunostar, cat# 20081):goat anti-5-HT antibody for 24hrs at 4°C abolished all staining of *Manduca* AL tissue (Fig. 1B). Non-pre-adsorbed controls in which goat anti-5-HT antibody was incubated in parallel under identical conditions with the exception of the 5-HT-BSA conjugate resulted in strong immunolabeling (Fig. 1C). For immunocytochemistry, tissue was incubated at a dilution of 1:10,000 for 24 hours.

***MsTH - Manduca sexta* tyrosine hydroxylase (MsTH)—**The MsTH antibody was raised in rabbit against MsTH, which is the rate limiting enzyme in the synthesis of DA. This antibody was generously provided by Dr. Maureen Gorman. The MsTH antibody was

raised against the full length MsTH protein and immunoblot analysis reveals a single band at the predicted height (Gorman et al., 2007). AL labeling with this antibody matches immunolabeling for DA with the exception of very weak labeling to an unknown substance that is not observed within glomeruli (Dacks et al., 2012). Tissue was incubated at a dilution of 1:5,000 for 24 hours.

GABA—The GABA antibody was raised in rabbit against GABA coupled to BSA with paraformaldehyde and obtained from Sigma Aldrich (Sigma Aldrich, cat # A2052). Controls performed by Sigma reveal that the antibody binds to GABA in a dot blot assay and not to BSA. Pre-adsorption controls were performed by incubating the rabbit anti-GABA antiserum for 24hrs in blocking solution (1mg/ml BSA in PBSAT) with GABA (Sigma Aldrich, cat # A2129) at a ratio of 10:1 GABA:antiserum which abolished all staining in *Manduca* AL tissue (Fig. 1D). Non-pre-adsorbed controls in which rabbit anti-GABA antibody was incubated in parallel under identical conditions with the exception of GABA resulted in strong immunolabeling (Fig. 1E). For immunocytochemistry, tissue was incubated at a dilution of 1:500 for 48 hours.

Myoinhibitory peptide (MIP)—Antiserum raised in rabbit against MIP conjugated to thyroglobulin was produced by M. Eckert, Jena Germany and provided by C. Wegener, Marburg Germany (Predel et al., 2001). Pre-adsorption of the antiserum by incubating with 1mg/mL BSA and 10:1 synthetic MIP_{VI} (AWSALHGAWA): rabbit anti-MIP antibody for 24 hours at 4°C abolished all staining of *Manduca* AL tissue (Fig. 1F). *Manduca sexta*-MIP_{VI} has been shown to be present in adult *Manduca* ALs using mass spectrometry (Utz et al., 2007). Non-pre-adsorbed controls in which rabbit anti-MIP antibody was incubated in parallel under identical conditions with the exception of the synthetic MIP_{VI} resulted in strong immunolabeling (Fig. 1G). For immunocytochemistry, tissue was incubated for 48 hours at a dilution of 1:3000.

Allatotropin (ATR)—Antiserum raised in rabbit against *Manduca* allatotropin (Mas-AT, referred to in this paper as ATR) was kindly provided by Dr. J. Veenstra, University of Bordeaux, Talence, France; (Veenstra and Hagedorn, 1995). Specificity of Mas-AT antisera was tested previously in *Manduca* tissue (Veenstra and Hagedorn, 1995). Incubation of antisera for 1 hour at room temperature abolished all immunostaining in *Manduca* brain sections while pre-adsorption with FLRFamide, FMRFamide, and Dip-AST7 (all Sigma-Aldrich) for 1 hour at room temperature had no effect on immunostaining (Veenstra and Hagedorn, 1995). For immunocytochemistry, tissue was incubated for 48 hours at a dilution of 1:3000.

Allatostatin (AST)—Antiserum was raised (Reichwald et al., 1994) in rabbit against octadecapeptideallatostatin (Pratt et al., 1991), ASB2, (AYSYVSEYKALPVYNFGL-NH2) of *Diploptera punctata* and kindly provided by Dr. J. Veenstra, University of Bordeaux, Talence, France. Pre-adsorption controls revealed that the antisera against AKSYNFGLamide, a YXFGLamide identified from *Manduca*, recognizes AKSYNFGLamide, a form of allatostatin (AST) and other allatostatin-like peptides within

Manduca tissue (Davis et al., 1997). For immunocytochemistry, tissue was incubated for 48 hours at a dilution of 1:3,000.

Tachykinin (TKK)—Antiserum raised in rabbit against locust tachykinin II with bovine thyroglobulin with glutaraldehyde was kindly provided to us Dr. J. Veenstra, University of Bordeaux, Talence, France. Pre-adsorption of the antiserum by incubating with 1mg/mL BSA and 10:1 synthetic TKK1 (RAPMGFMGVR): rabbit anti-TKK antibody for 24hrs at 4°C abolished all staining of *Manduca* AL tissue (Fig. 1H). Non-pre-adsorbed controls in which rabbit anti-TKK antibody was incubated in parallel under identical conditions with the exception of the synthetic TKK_1 resulted in strong immunolabeling (Fig. 1I). For immunocytochemistry, tissue was incubated for 48 hours at a dilution of 1:4,000.

Confocal Microscopy—Images were scanned using an Olympus FV1000 confocal microscope with argon and green and red HeNe lasers. Fluoview software was used to adjust brightness levels, and Corel Draw 4.0 was used to organize figures.

Analysis

To quantify the relative distribution of each neuron type within a glomerulus we used two analytical approaches. The first approach was to determine the relative distance that each neuronal type projected along the proximal to distal axis of the glomerulus. The second approach was to make pair-wise comparisons of the distribution of each neuron type across the glomerulus to determine the similarity of their distribution. These approaches are depicted in Figure 2.

For each glomerulus analyzed, .tif stacks of AL scans were converted into an RBG color scheme in Fluoview software and imported into Corel Draw 4.0. Glomeruli were marked with a white dot at their most proximal, central point (Figure 2A) and cropped using the BRP staining as the boundary of glomerular area. Glomeruli were then oriented such that the white dot was at the bottom-most or “6 o’ clock” position. This was to ensure that horizontal bin 1 always corresponds to the most proximal end of the glomerulus and horizontal bin 10 to the most distal (Fig. 2B). A white bordered square with edges flush to the cropped glomerulus was applied (square shown with black border in figure 2B to visualize concept). Each cropped glomerulus and white square was exported individually as a .tif file and imported into MatLAB. Intensity values for each channel were extracted and all values that fell within the white square, but not within the glomerulus, were assigned a value of “not a number”, and thus excluded from analysis. The square was then divided into a 10×10 matrix (Fig. 2C), however, given the non-square structure of glomeruli, not all rows or columns contained a pixel number divisible by 10, and therefore the unequal bin sizes were randomly assigned to a bin(s). For example, one glomerulus may be 756 pixels in height by 654 pixels in width. To divide the glomerulus into 10 rows, 756 pixels are distributed into 6 rows that are 76 pixels in height and 4 rows that are 75 pixels in height. Thus, the rows are randomly assigned to having 76 vs. 75 pixels. The intensity values from each bin in a glomerulus were then normalized by subtracting each bin by the minimum fluorescence divided by the maximum fluorescence minus the minimum fluorescence for that glomerulus $((X - X_{min})/(X_{max}-X_{min}))$. Figure 2 D&E are intensity maps of two separate channels (MsTH-ir and 5-

HT-ir for figures 2D and E respectively) from a single glomerulus run through the intensity analysis to demonstrate how each immunolabel exhibits varying levels of pixel intensities across the 10×10 grid.

For the relative distance analysis, we averaged row values in our 10×10 grid to get a resolution of 10 horizontal bins for intensity values. We used the normalized intensity values for each resulting horizontal bin (1 being most proximal, 10 most distal) for each neuron to compare the distance they extend within a glomerulus. A 1-way ANOVA for each neuron type was performed to determine at what point along the proximal to distal axis the pixel intensity values began to significantly reduce relative to the point of entry to the glomerulus. For all neuron types, with the exception of ORNs, the comparison was with relation to the proximal end of the glomerulus.

For the pair-wise correlational analysis, we calculated average normalized intensity values across our 10×10 grid of glomeruli and then plotted the intensity values as heatmaps using the heatmap function in MatLAB (available at http://www.mathworks.com/matlabcentral/?refresh=true). To quantify the similarity in glomerular distribution between labeling groups, i.e. ORN vs. PN, we ran a pair-wise linear regression analysis using Graph Pad Prism v.6.01 (Graphpad Software Incorporated) to obtain a linear relationship and R^2 values for each possible combination of neuron type and immunostain. We note, the purpose of our correlation analysis was not to demonstrate whether each neuron type synapses with each other, but rather, to establish a predictive relationship determining that if ‘x’ appears in bin 10, how often will ‘y’ appear in that same bin at a similar level of intensity.

For 5-HT and MsTH, 100 sexually isomorphic glomeruli from 10 moths were used. To directly compare the intensity values for 5-HT-ir and MsTH-ir at each bin we used multiple T-tests with the Holm-Sidak method to correct for multiple comparisons in Graphpad Prism. For ORNs, PNs and GABA 10 sexually isomorphic glomeruli from 5 animals for each neuron type were used. The analyses were performed in duplicate by two different individuals on different computers and the results were consistent and reliable across person.

All references to neuroanatomical structures use the terminology set out in Ito et al. (2014). The goal of this study is to determine the relative distribution of two extrinsic neuromodulatory neurons in relation to the primary neuron types of the AL. We do not assume connectivity based on overlap of projections, rather we are using relative distribution to provide a framework for studying the convergence of neuromodulatory inputs to this sensory network.

Results

The AL receives serotonergic and dopaminergic input from two separate sets of extrinsic neurons. The contralaterally projecting serotonin-immunoreactive deutocerebral neuron (CSD) (Kent et al., 1987; Dacks et al., 2006a) and dopaminergic arching neurons (DAAR) (Dacks et al., 2012) project widely throughout the brain (schematized in Fig. 3A) and innervate every glomerulus of the AL. One CSD neuron cell body resides in each lateral cell cluster of the AL, projects along the medial antennal lobe tract (mALT) to the superior

protocerebrum where it crosses the midline and projects anteriorly to innervate all glomeruli of the contralateral AL after having innervated both lateral horns and other protocerebral regions (Kent et al., 1987). There are two pairs of DAAR neurons, each of which projects to lateral protocerebral regions on each side of the brain as well as to both ALs where they innervate all glomeruli (Dacks et al., 2012). Thus each AL receives input from a single CSD neuron and four DAAR neurons.

CSD and DAAR neurons innervate distinct yet overlapping glomerular zones

To determine the extent of overlap between the serotonergic and dopaminergic systems within glomeruli, we labeled for 5-HT, MsTH, and BRP in adult moths. MsTH was used to immunolabel the dopaminergic DAAR neurons and the BRP antibody was used to delineate glomerular boundaries. In sexually isomorphic glomeruli, MsTH-ir extends farther distally than 5-HT which remains proximal relative to the center of the AL (Fig. 3B-D). Using multiple t tests, we found that the distribution of 5-HT and DA significantly differed for the most distal bins 7-10, bin 1 being most proximal and bin 10 most distal (Fig. 3E; Multiple t-tests; t= 2.76 for bin7, t=4.55 for bin 8, t= 5.44 for bin 9, t= 4.68 for bin 10; df=18; p=0.012 for bin 7p<0.0001 for bin 8-10; n=100). Using a 1-way ANOVA to make within modulator comparisons of intensity, we also sought to define where the distribution of each modulator began to significantly reduce in intensity along the proximal to distal axis. To determine at what point along the proximal to distal axis 5-HT-ir and MsTH-ir began to differ in intensity we used a 1-way ANOVA to compare intensity levels between each bin. The intensity values of the 5-HT-ir began to significantly decrease at bin 6 (Fig. 3E_, p<0.01, df=9, n=10), while the MsTH-ir intensity values do not significantly decrease until bin 9 (Fig. 3E, p<0.05, df=9, n=10). *Manduca* possess three sexually dimorphic glomeruli, which comprise the macroglomerular complex (MGC) in males and receive input from ORNs responsive to components of the female sex pheromone (Christensen and Hildebrand, 1987). In the MGC, MsTH also extends farther distally than 5-HT (Fig. 3F) although neither biogenic amine extended as far distally in the MGC as in the isomorphic glomeruli.

In many invertebrates, the axon terminals of ORNs innervate the distal portion of glomeruli, whereas the processes of PNs and LNs are more proximal (as reviewed in Ache and Young, 2005). To quantitatively illustrate the distribution of the three principal neuron types along the proximal to distal axis of a glomerulus in *Manduca*, in separate groups of moths we labeled ORNs via anterograde dye fills from the antennae, PNs via retrograde dye fills from the mushroom bodies and GABA-ir LNs and PNs via immunolabeling for GABA. Dye filled PNs and GABA-ir neurons had the greatest intensity within the most proximal 5 bins of the glomerulus, while dye filled ORNs were greatest in intensity in the most distal portion of a glomerulus (bins 7-10) (Fig. 4A). To determine at what point along the proximal to distal axis each of the 3 neuronal types began to differ in intensity, we used a 1-way ANOVA to compare intensity levels between each bin for each individual neuron type. ORN intensity values began to significantly decrease relative to the most distal bin at bin 6 (Fig. 4A, p<0.05, df=9, n=10), PN intensity values began to significantly decrease relative to the most proximal bin at bin 9 (Fig. 4A, p<0.05, df=9, n=10) and GABA intensity values began to significantly decrease relative to the most proximal bin at bin 5 (Fig. 4A, p<0.01, df=9, n=10).

Glomeruli are irregular spheroidal structures, thus using a 10×10 grid of intensity across vertical and horizontal bins was necessary to capture the unique distribution pattern of each neuron type. In *Manduca*, ORNs do not innervate the glomerulus in a perfect linear progression along the distal to proximal axis, but rather form a crescent around the distal glomerular half (Fig. 4B). Conversely, PNs and GABA-ir AL neurons occupy a proximal "spheroid" within the crescent formed by the ORNs (Fig. 4C, D). To quantify the degree of similarity between these general distributions we ran a pair-wise linear regression analysis of the labeling intensity for each neuronal type within a glomerulus. The innervation patterns of ORNs and PNs showed a significant negative relationship (Fig. 4E; $r^2 = 0.3251$, $p<0.0001$) as did the patterns for ORNs and GABA (Fig. 4F; $r^2 = 0.6494$, $p<0.0001$). Finally, the innervation patterns of PNs and GABA-ir AL neurons showed a significant positive relationship (Fig. 4G; $r^2 = 0.2444$, $p<0.0001$).

We therefore sought to determine if the differences in innervation pattern of the CSD and DAAR neurons were reflective of differences in the glomerular regions occupied by the ORNs, LNs and PNs. Antennal nerve fills were used to anterogradely fill the axons of ORNs to the AL (Fig. 5A). Subsequent immunocytochemical labeling for 5-HT and MsTH revealed that, consistent with Sun et al. (1993), the 5-HT-ir processes remained proximal and had little overlap with the ORNs (Fig. 3B), while ORNs almost completely overlapped with MsTH-ir (Fig. 3C). An almost complete lack of overlap between 5-HT-ir and ORNs was also observed in the MGC (Fig. 3D-F). Using a 10×10 grid of intensity across vertical and horizontal bins to determine the average distribution of ORNs, 5-HT-ir and MsTH-ir, we found that ORNs occupy the most distal bins as shown in (Fig. 5G), while 5-HT-ir and MsTH-ir both innervate the most proximal bins (Fig. 5H-I) with MsTH-ir extending farther distally into the glomerulus (Fig. 5I). To quantify the degree of similarity between ORNs and 5-HT-ir we ran a pair-wise linear regression analysis of the labeling intensity for each neuronal type within a glomerulus. Both 5-HT-ir and MsTH-ir showed a negative relationship with ORNs (Fig. 5J-K; $r^2 = 0.6162$, $p<0.0001$ and $r^2 = 0.5133$, $p<0.0001$ respectively). To illustrate the distribution of the CSD and DAAR processes relative to PN dendrites, mushroom body dye fills were used to retrogradely fill PN processes in the AL (Fig. 6A). The CSD and DAAR processes intermingle with PN dendrites, but only the DAAR neurons extend more distally beyond the boundary of the PNs (Figure 4B-G). Both 5-HT-ir and MsTH-ir showed a positive relationship with PNs (Fig. 6E-F; $r^2 = 0.2810$, $p<0.0001$, $r^2 = 0.09240$, $p = 0.0022$ respectively).

Distribution of the CSD and DAAR neurons relative to the GABAergic and peptidergic AL neurons

To illustrate the relative distribution of the CSD processes with the diverse modulatory environment of the AL, we compared the distribution of 5-HT-ir to the intrinsic modulatory network of GABAergic and peptidergic AL neurons in the lateral cell cluster. Because the most reliable GABA antibody and all of the available neuropeptide antibodies were raised in rabbit, we did not examine their relative distribution with MsTH-ir as this antibody was also raised in rabbit. There are ~460 GABAergic cell bodies in the lateral cell cluster, of which 360 are LNs and 100 are PNs (Hoskins et al., 1986), so GABA-ir provides a method to highlight a major proportion of cells in the lateral cell cluster of *Manduca*. Consistent with

(Hoskins et al., 1986), GABA-ir processes were denser at the proximal region of isomorphic glomeruli and sparser distally (Fig. 4A&D). Triple immunolabeling (Fig. 7A) revealed extensive overlap of 5-HT-ir within the denser GABA-ir in the proximal region of the isomorphic glomeruli (Fig. 7B). As in Figure 3, the BRP antibody was used to delineate glomerular boundaries. However, the CSD neurons did not extend their processes distally past the boundary at which the GABA-ir processes become spare (Fig. 7C, D). GABA showed a significant positive relationship with 5-HT (Fig. 7E; $r^2 = 0.4436$, $p<0.0001$).

Despite the large number of GABAergic LNs, not all LNs in the ALs of *Manduca* are GABAergic (Reisenman et al., 2011) and many LNs (and some PNs) express a variety of different neuropeptides (Homberg et al., 1990; Utz and Schachtner, 2005; Reisenman et al., 2011). Thus, antibodies against several neuropeptides were used to highlight the processes of a smaller number of LNs and PNs than are labeled with GABA-ir. Figure 8 depicts the arborizations of the CSD neuron and 4 populations of peptidergic neurons: tachykinin-ir (TKK; Fig. 8A-F), allatotropin-ir (ATR; Fig. 8G-I), allatostatin-ir (AST; Fig. 8J-L) and myoinhibitory peptide-ir (MIP; Fig. 8M-P). Within the isomorphic glomeruli (Fig. 8; central column) all four populations of peptidergic neurons overlap with 5-HT-ir but all extend farther distally. To the best of our knowledge, this is the first description of TKK-ir in the AL of *Manduca*. Each AL possesses ~9 TKK-ir cell bodies which together innervate all glomeruli (Fig. 8A-B). While some TKK-ir cell bodies appear to be LNs according to their morphology, there is a process leaving the AL (Fig. 8C), demonstrating that some TKK-ir cells may be PNs or even centrifugal neurons. A small number of ATR-ir neurons in the lateral cell cluster are also PNs and a few centrifugal AST-ir neurons innervate the AL and arborize in glomeruli (Utz and Schachtner, 2005; Utz et al., 2007; Utz et al., 2008). Similar to the GABA-ir, ATR-ir was denser at the proximal core of isomorphic glomeruli as well as the MGC, but did extend distally with sparer processes (Fig 8I). The AST-ir was also denser proximally, although not nearly to the same extent as the GABA-ir or the ATR-ir (Fig. 8K). MIP-ir and TKK-ir were generally uniform in density. Utz et al., 2007 reported that the majority of MIP-ir neurons are LNs based on their morphology, and our results were consistent with this finding in that the MIP-ir cell bodies were relatively large, on average ~20 um compared to PN cell bodies in the lateral cell cluster (6.2-8.9um; Homberg et al., 1988). MIP-ir was uniformly distributed throughout isomorphic glomeruli, extending farther distally than 5-HT in both the isomorphic glomeruli and the MGC (Fig. 8N-O).

Discussion

Neuromodulation provides a network with the capacity to produce a wide range of output under different conditions. Without this flexibility the same network would need exponentially more connections to achieve the same endpoint. A variety of external and internal conditions trigger the release of neuromodulators and as a consequence each network must dynamically integrate the influences of many neuromodulators. In this study, we described the relative glomerular distribution of two extrinsic modulatory systems within the AL of *Manduca*, their overlap with input neurons, output neurons and intrinsic sources of neuromodulators. The differences in the glomerular arborizations of the CSD and DAAR neurons (releasing 5-HT and DA respectively) suggest that each modulator targets partially overlapping functional groups of neurons. While both the processes of the CSD and DAAR

neurons overlap extensively with LNs and PNs, the DAAR neurons extended sufficiently distally to overlap with the axon terminals of ORNs while the CSD neurons remained proximal and had very little overlap with ORNs. Based on their anatomical distributions within glomeruli, the CSD neurons are less likely to have significant presynaptic influence on ORNs while the DAAR neurons have the potential to influence all three major intrinsic neuron types in the AL.

We employed two approaches to analyze the distribution of 5-HT-ir and MsTH-ir with each other and with the three major AL neuron types. To determine if CSD and DAAR neurons differ in the distance that they extend within a glomerulus, we divided glomeruli into 10 bins along the proximal to distal axis and made comparisons of immunolabeling intensity at each bin. This allowed us to determine that these two modulatory populations had similar levels of innervation of the proximal glomerular regions, but differed in their distribution within the distal region. Specifically, the intensity values for 5-HT-ir began to significantly decrease within the distal 40% of the glomerulus, while MsTH-ir did not significantly decrease until the distal 20% of the glomerulus (Fig. 3E). Although their decrease was much more gradual than that of the 5-HT-ir, PNs and GABA-ir neurons also decreased in their innervation in the distal glomerular region (Fig. 4A). ORNs, on the other hand had their greatest intensity within the distal 40% of the glomeruli and decreased proximally. Pair-wise comparisons of each neuronal type revealed that overall, ORNs typically showed a negative relationship with the other neuronal types (Figs. 4E,F and 5J,K), whereas all other pair-wise comparisons showed a positive relationship. Despite the negative relationship of overall distribution of MsTH-ir with ORNs across the entire glomerulus, MsTH-ir neurons had a higher intensity than 5-HT-ir, PNs and GABA-ir neurons within the distal most regions of the glomerulus occupied by the ORNs (Fig. 3E and 4A).

While overlapping projections converging in the same glomerular sub-region suggest potential interaction of neuromodulators, anatomy is only the first step in determining a basis for the convergent physiological effects of neuromodulation. The physiological convergence of neuromodulators depends upon receptor expression of the pre or postsynaptic neuron. Consistent with our finding that the distributions of 5-HT-ir and GABA-ir overlapped, GABAergic LNs within the AL of *Manduca* express the Ms5HT1A receptor (Dacks et al., 2013) and presumed LNs grown in cell culture, and therefore isolated from any synaptic input, are directly modulated by 5-HT (Mercer et al 1995). Ms5HT1B, Ms5HT2 and Ms5HT7 receptor mRNAs are expressed in the AL (Dacks et al., 2006b; Dacks et al., 2013) as are the mRNAs for the MsDop1, MsDop2 and MsINDR receptors (Dacks et al., 2012). However, receptor expression by specific neuronal types of the AL (i.e. LN vs. PN) of *Manduca* is still relatively unexplored. Receptors for 5-HT and DA have the capacity to converge upon the same biochemical cascades as they all couple to adenylyl cyclase to affect cAMP levels (Saudou et al., 1992; Colas et al., 1995; Mustard et al., 2005). However, the biochemical consequences of activating 5-HT and DA receptors also have the opportunity to diverge, as the 5-HT1 and 5-HT2 receptor subtypes affect IP_3 pathways while DA receptors and the 5-HT7 receptor do not (Saudou et al., 1992; Mustard et al., 2005).

The potential for convergent modulatory influence is present in all insect ALs. Most, if not all glomeruli receive input from 5-HT (Kent et al., 1987; Salecker and Distler, 1990; Sun et

al., 1993; Wegerhoff, 1999; Hill et al., 2002; Dacks et al., 2006a; Roy et al., 2007) and neuropeptides (Carlsson et al., 2010; Kromann et al., 2013; Siju et al., 2013) suggesting that neuromodulation is ubiquitous within the AL. In the AL of *Manduca*, the CSD and DAAR neurons both ramify in all glomeruli (Kent et al., 1987; Dacks et al., 2006a; Dacks et al., 2012) however, we demonstrate their relative projection patterns reveal the potential for convergent modulation on LNs and PNs and differences in their ability to presynaptically modulate ORNs. This is consistent with work in *Drosophila* showing that presynaptic inhibition of ORNs by GABAergic LNs is enhanced by 5-HT despite 5-HT having no direct effect on ORNs (Dacks et al., 2009). This suggests that 5-HT acts, in part, through lateral interactions exerted by LNs to shape odor evoked responses. Furthermore, the glomeruli to which the CSD neurons project in the AL of *Drosophila* are tightly regulated by ephrin signaling pathways and the disruption of this developmental control has significant consequences for odor-guided behavior (Singh et al., 2013). This suggests that the stereotyped distribution of CSD processes has functional consequences for odor-processing. In *Manduca*, 5-HT has odor specific effects on AL neuron responses, further suggesting that 5-HT modulates the capacity of LNs to refine the transfer of information between ORNs and PNs (Dacks et al., 2008). However, this does not suggest that ORNs are not affected by 5-HT from sources other than the CSD neurons. ORNs are continuously subjected to the influence of circulating neuromodulators in the hemolymph (Schendzielorz et al., 2015) and the mRNA for four of the *Manduca* 5-HT receptors are expressed in the antennae, far from the axons of CSD neurons in the AL (Dacks et al., 2006b; Dacks et al., 2013), although it is possible that 5-HT release from the CSDs may act at a distance to influence ORNs in an as yet unobserved manner.

Although 5-HT and DA are likely released under different behavioral contexts, they both generally enhance odor evoked responses of AL neurons (Kloppenburg and Hildebrand, 1995; Dacks et al., 2008; Kloppenburg and Mercer, 2008; Dacks et al., 2012), although their effects differ in several ways. The levels of 5-HT in the ALs of *Manduca* fluctuate throughout the day peaking at dawn and dusk (Kloppenburg et al., 1999), when *Manduca* perform the majority of their odor-guided behaviors (Lingren et al., 1977). Furthermore, injection of 5-HT into cabbage looper moths broadens the range of the day in which male moths will fly to female pheromone (Linn and Roelofs, 1986). This suggests that the release of 5-HT by the CSD neurons is at least, in part, regulated by the waking state. Physiologically, bath application of 5-HT reduces two K^+ conductances, a sustained I_{KV}-like conductance and a more transient I_A-like conductance, and lowers the voltage of inactivation for the I_A-like conductance in PNs (Kloppenburg et al., 1999) and cultured LNs (Mercer et al., 1995). As a consequence, the resistance (and therefore the excitability) of LNs and PNs is increased by 5-HT (Kloppenburg and Hildebrand, 1995) and the odor-evoked responses of AL neurons is also increased (Kloppenburg et al., 1999; Dacks et al., 2008). Another consequence of the effects 5-HT is an increase in the slope of odor-evoked responses as a function of odor concentration (Dacks et al., 2008) suggesting that 5-HT modulates the gain of the AL.

The context for the release of DA within the AL is associated with the context of aversive stimuli, as injection of DA receptor antagonists into the ALs blocks aversive conditioning (Dacks et al., 2012), but not appetitive conditioning (Riffell et al., 2013). Similar to 5-HT,

bath application of DA increased the maximal odor-evoked firing rate of extracellularly recorded AL neurons, but did not affect response gain (Dacks et al., 2012) as was observed for 5-HT (Dacks et al., 2008). DA and 5-HT also differ in their effects on the temporal dynamics of odor evoked responses. While 5-HT generally increased odor evoked response duration (Kloppenburg et al., 1999; Dacks et al., 2008), DA reduced the post-excitation period of spike suppression in PNs called the I_2 phase (Dacks et al., 2012) that typically lasts between 10ms and 1.5 seconds (Christensen et al., 1996). The I_2 phase affects the fidelity with which PNs can encode the temporal dynamics of odor stimuli and blocking the I_2 phase altogether negatively impacts the ability of moths to track odor plumes (Lei et al., 2009), suggesting that DA may modulate the coding of stimulus timing within the AL. Although the physiological effects of both modulators on a single AL neuron have not been examined, ~50% of AL neurons are affected by 5-HT (Kloppenburg and Hildebrand, 1995; Mercer et al., 1995; Dacks et al., 2008) and ~60% of AL neurons are affected by DA (Dacks et al., 2012), suggesting that at least 10% of AL neurons are affected by both modulators. The AL must therefore integrate the effects of multiple neuromodulators, which each have distinct effects information processing and sensory coding.

Neuromodulatory neurons can be extrinsic (projecting from outside the network) or intrinsic (part of the network) to a system (Katz, 1999). In the AL, LNs intrinsic to the network refine the transfer of information from ORNs to PNs via a diverse set of pre- and post-synaptic mechanisms. In *Manduca*, GABAergic LNs mediate a variety of tasks including maintaining temporal fidelity, contrast enhancement between glomeruli and intraglomerular and interglomerular synchrony (Waldrop et al., 1987; Christensen et al., 1998; Lei et al., 2002; Lei et al., 2009; Tripathy et al., 2010; Daly et al., 2011; Martin et al., 2011). Furthermore, LNs co-express a diverse array of neuropeptides for which a few have been demonstrated to modulate olfactory processing (Ignell et al., 2009; Root et al., 2011). In *Drosophila*, LNs co-transmit GABA and tachykinin (Carlsson et al., 2010), both of which mediate presynaptic gain control of ORNs via GABAb receptors (Olsen and Wilson, 2008; Root et al., 2008) and tachykinin receptors (Ignell et al., 2009). Unlike classical small neurotransmitters such as GABA, neuropeptides work on at least a 100-fold longer time scale (Salio et al., 2006). Thus, the co-release of both GABA and neuropeptides in *Manduca* may provide layers of inhibition exerted over different time courses. While LNs represent a source of neuromodulation exerted within the context of recent network activation, the CSD and DAAR neurons represent an extrinsic source of neuromodulation exerted based on the general physiological state of the individual moth. All of these neuromodulatory neurons had a high degree of overlap (Fig. 3, 8) within the glomeruli suggesting that olfactory processing is dynamically shaped by multiple modulatory inputs, both extrinsic and intrinsic.

Sensory systems adjust how they encode information about the environment under a variety of different circumstances. Different internal and external conditions exert constraints on the physiological needs of the individual animal and the capacity to modify sensory processing in an appropriate manner is, in part, carried out by the integration of multiple sources of modulation. The integration of multiple modulators within a single network, neuron or second messenger pathway allows dynamic control over biophysical properties and vesicle release on both short and long time scales potentially with non-linear effects. In this manner,

integrated modulation increases cellular dynamics, expanding the processing power of a network. Our data reveals that 5-HT and DA may converge upon the same neuron types, providing the potential for their integrated effects. Intrinsic and extrinsic modulatory neurons represent a significant proportion of the AL network which speaks to the importance of neuromodulation for information processing within the AL. Overall, the integration of modulators within the olfactory system may serve as a layered source of modulation for dynamically adjusting sensory processing in a complex, odor filled environment.

Acknowledgments

We would like to thank Jing Wang for helping with data collection support, as well as the other members of the Dacks lab for their support. The TKK, AST, and ATR antibodies were provided by Dr. Jan Veenstra, the MIP antibody was provided by Dr. Christian Wegener and developed by Dr. Manfred Eckert and the MsTH antibody by Dr. Maureen Gorman. This work was supported by start-up funds from West Virginia University and a R03 DC013997-01 from the National Institutes of Health to AMD. We thank Dr. Kevin Daly, Dr. Sarah Farris and Tyler Sizemore for providing critical feedback on earlier versions of this manuscript.

Role of Authors: All authors had full access to all the data in the study and take responsibility for the integrity of the data and the accuracy of the data analysis. Study concept and design: Kristyn M. Lizbinski (KML), Jackie D. Metheny (JDM), Andrew M. Dacks (AMD). Acquisition of data: KML, JDM. Analysis and interpretation of data: KML, JDM, Aditya Kesari (AK), Samual P. Bradley (SPB). Drafting of the manuscript: KML, AMD. Critical revision of the manuscript for important intellectual content: KML, AK, JDM, SPB, AMD. Statistical analysis: KML, SPB, AK, AMD. Obtained funding: AMD Administrative, technical, and material support: AMD. Study supervision: AMD

Works Cited

Ache BW, Young JM. Olfaction: diverse species, conserved principles. Neuron. 2005; 48(3):417–430. [PubMed: 16269360]

Bargmann CI. Beyond the connectome: how neuromodulators shape neural circuits. Bioessays. 2012; 34(6):458–465. [PubMed: 22396302]

Bell RA, Joachim FG. Techniques for Rearing Laboratory Colonies of Tobacco Hornworms and Pink Bollworms Lepidoptera-Sphingidae-Gelechiidae. Ann Entomol Soc Am. 1976; 69(2):365–373.

Brezina V. Beyond the wiring diagram: signalling through complex neuromodulator networks. Philos Trans R Soc Lond B Biol Sci. 2010; 365(1551):2363–2374. [PubMed: 20603357]

Carlsson MA, Diesner M, Schachtner J, Nassel DR. Multiple neuropeptides in the Drosophila antennal lobe suggest complex modulatory circuits. J Comp Neurol. 2010; 518(16):3359–3380. [PubMed: 20575072]

Champagne MB, Edwards KA, Erickson HP, Kiehart DP. Drosophila stretchin-MLCK is a novel member of the Titin/Myosin light chain kinase family. J Mol Biol. 2000; 300(4):759–777. [PubMed: 10891286]

Christensen TA, Heinbockel T, Hildebrand JG. Olfactory information processing in the brain: encoding chemical and temporal features of odors. J Neurobiol. 1996; 30(1):82–91. [PubMed: 8727985]

Christensen TA, Hildebrand JG. Male-specific, sex pheromone-selective projection neurons in the antennal lobes of the moth Manduca sexta. J Comp Physiol A. 1987; 160(5):553–569. [PubMed: 3612589]

Christensen TA, Waldrop BR, Hildebrand JG. Multitasking in the olfactory system: context-dependent responses to odors reveal dual GABA-regulated coding mechanisms in single olfactory projection neurons. J Neurosci. 1998; 18(15):5999–6008. [PubMed: 9671685]

Colas JF, Launay JM, Kellermann O, Rosay P, Maroteaux L. Drosophila 5-HT2 serotonin receptor: coexpression with fushi-tarazu during segmentation. Proc Natl Acad Sci U S A. 1995; 92(12): 5441–5445. [PubMed: 7777527]

Dacks AM, Christensen TA, Hildebrand JG. Phylogeny of a serotonin-immunoreactive neuron in the primary olfactory center of the insect brain. J Comp Neurol. 2006a; 498(6):727–746. [PubMed: 16927264]

Dacks AM, Christensen TA, Hildebrand JG. Modulation of olfactory information processing in the antennal lobe of Manduca sexta by serotonin. J Neurophysiol. 2008; 99(5):2077–2085. [PubMed: 18322001]

Dacks AM, Dacks JB, Christensen TA, Nighorn AJ. The cloning of one putative octopamine receptor and two putative serotonin receptors from the tobacco hawkmoth, Manduca sexta. Insect Biochem Mol Biol. 2006b; 36(9):741–747. [PubMed: 16935223]

Dacks AM, Green DS, Root CM, Nighorn AJ, Wang JW. Serotonin modulates olfactory processing in the antennal lobe of Drosophila. J Neurogenet. 2009; 23(4):366–377. [PubMed: 19863268]

Dacks AM, Reale V, Pi Y, Zhang W, Dacks JB, Nighorn AJ, Evans PD. A Characterization of the Manduca sexta Serotonin Receptors in the Context of Olfactory Neuromodulation. PLoS One. 2013; 8(7):e69422. [PubMed: 23922709]

Dacks AM, Reisenman CE, Paulk AC, Nighorn AJ. Histamine-immunoreactive local neurons in the antennal lobes of the hymenoptera. J Comp Neurol. 2010; 518(15):2917–2933. [PubMed: 20533353]

Dacks AM, Riffell JA, Martin JP, Gage SL, Nighorn AJ. Olfactory modulation by dopamine in the context of aversive learning. J Neurophysiol. 2012; 108(2):539–550. [PubMed: 22552185]

Daly KC, Galan RF, Peters OJ, Staudacher EM. Detailed Characterization of Local Field Potential Oscillations and Their Relationship to Spike Timing in the Antennal Lobe of the Moth Manduca sexta. Frontiers in neuroengineering. 2011; 4:12. [PubMed: 22046161]

Daly KC, Kalwar F, Hatfield M, Staudacher E, Bradley SP. Odor detection in Manduca sexta is optimized when odor stimuli are pulsed at a frequency matching the wing beat during flight. PLoS One. 2013; 8(11):e81863. [PubMed: 24278463]

Davis NT, Veenstra JA, Feyereisen R, Hildebrand JG. Allatostatin-like-immunoreactive neurons of the tobacco hornworm, Manduca sexta, and isolation and identification of a new neuropeptide related to cockroach allatostatins. J Comp Neurol. 1997; 385(2):265–284. [PubMed: 9268127]

Fontanini A, Katz DB. State-dependent modulation of time-varying gustatory responses. J Neurophysiol. 2006; 96(6):3183–3193. [PubMed: 16928791]

Getting PA. Emerging principles governing the operation of neural networks. Annu Rev Neurosci. 1989; 12:185–204. [PubMed: 2648949]

Gorman MJ, An C, Kanost MR. Characterization of tyrosine hydroxylase from Manduca sexta. Insect Biochem Mol Biol. 2007; 37(12):1327–1337. [PubMed: 17967351]

Hill ES, Iwano M, Gatellier L, Kanzaki R. Morphology and physiology of the serotonin-immunoreactive putative antennal lobe feedback neuron in the male silkmoth Bombyx mori. Chem Senses. 2002; 27(5):475–483. [PubMed: 12052784]

Homberg U, Kingan TG, Hildebrand JG. Distribution of FMRFamide-like immunoreactivity in the brain and suboesophageal ganglion of the sphinx moth Manduca sexta and colocalization with SCPB-, BPP-, and GABA-like immunoreactivity. Cell Tissue Res. 1990; 259(3):401–419. [PubMed: 2180574]

Homberg U, Montague RA, Hildebrand JG. Anatomy of antenno-cerebral pathways in the brain of the sphinx moth Manduca sexta. Cell Tissue Res. 1988; 254(2):255–281. [PubMed: 3197087]

Hoskins SG, Homberg U, Kingan TG, Christensen TA, Hildebrand JG. Immunocytochemistry of GABA in the antennal lobes of the sphinx moth Manduca sexta. Cell Tissue Res. 1986; 244(2): 243–252. [PubMed: 3521878]

Huetteroth W, Schachtner J. Standard three-dimensional glomeruli of the Manduca sexta antennal lobe: a tool to study both developmental and adult neuronal plasticity. Cell Tissue Res. 2005; 319(3): 513–524. [PubMed: 15672266]

Hurley LM, Hall IC. Context-dependent modulation of auditory processing by serotonin. Hearing research. 2011; 279(1-2):74–84. [PubMed: 21187135]

Ignell R, Root CM, Birse RT, Wang JW, Nassel DR, Winther AM. Presynaptic peptidergic modulation of olfactory receptor neurons in Drosophila. Proc Natl Acad Sci U S A. 2009; 106(31):13070–13075. [PubMed: 19625621]

Ito K, Shinomiya K, Ito M, Armstrong JD, Boyan G, Hartenstein V, Harzsch S, Heisenberg M, Homberg U, Jenett A, Keshishian H, Restifo LL, Rossler W, Simpson JH, Strausfeld NJ, Strauss R, Vosshall LB, Insect Brain Name Working G. A systematic nomenclature for the insect brain. Neuron. 2014; 81(4):755–765. [PubMed: 24559671]

Kaczmarek, LK.; Levitan, IB. Neuromodulation: the biochemical control of neuronal excitability. Oxford University Press; New York: 1987. p. ixp. 286

Katz, PS. Beyond neurotransmission: neuromodulation and its importance for information processing. Oxford University Press; Osford; New York: 1999. p. xiiip. 391

Kent KS, Hoskins SG, Hildebrand JG. A novel serotonin-immunoreactive neuron in the antennal lobe of the sphinx moth Manduca sexta persists throughout postembryonic life. J Neurobiol. 1987; 18(5):451–465. [PubMed: 3309187]

Kloppenburg P, Ferns D, Mercer AR. Serotonin enhances central olfactory neuron responses to female sex pheromone in the male sphinx moth manduca sexta. J Neurosci. 1999; 19(19):8172–8181. [PubMed: 10493719]

Kloppenburg P, Heinbockel T. 5-Hydroxy-tryptamine modulates pheromone-evoked local field potentials in the macroglomerular complex of the sphinx moth Manduca sexta. J Exp Biol. 2000; 203(Pt 11):1701–1709. [PubMed: 10804160]

Kloppenburg P, Hildebrand JG. Neuromodulation by 5-hydroxytryptamine in the antennal lobe of the sphinx moth Manduca sexta. J Exp Biol. 1995; 198(Pt 3):603–611. [PubMed: 7714450]

Kloppenburg P, Mercer AR. Serotonin modulation of moth central olfactory neurons. Annu Rev Entomol. 2008; 53:179–190. [PubMed: 18067443]

Komuniecki R, Hapiak V, Harris G, Bamber B. Context-dependent modulation reconfigures interactive sensory-mediated microcircuits in Caenorhabditis elegans. Curr Opin Neurobiol. 2014; 29:17–24. [PubMed: 24811318]

Kromann SH, Hansson BS, Ignell R. Distribution of neuropeptides in the antennal lobes of male Spodoptera littoralis. Cell Tissue Res. 2013

Kupfermann I. Modulatory actions of neurotransmitters. Annu Rev Neurosci. 1979; 2:447–465. [PubMed: 44174]

Lei H, Christensen TA, Hildebrand JG. Local inhibition modulates odor-evoked synchronization of glomerulus-specific output neurons. Nat Neurosci. 2002; 5(6):557–565. [PubMed: 12006983]

Lei H, Riffell JA, Gage SL, Hildebrand JG. Contrast enhancement of stimulus intermittency in a primary olfactory network and its behavioral significance. J Biol. 2009; 8(2):21. [PubMed: 19232128]

Lingren PD, Greene GL, Davis DR, Baumhover AH, Henneberry TJ. Nocturnal Behavior of 4 Lepidopteran Pests That Attack Tobacco and Other Crops. Ann Entomol Soc Am. 1977; 70(2): 161–167.

Linn CE, Roelofs WL. Modulatory Effects of Octopamine and Serotonin on Male Sensitivity and Periodicity of Response to Sex-Pheromone in the Cabbage-Looper Moth, Trichoplusia-Ni. Arch Insect Biochem. 1986; 3(2):161–171.

Marder E. Neuromodulation of neuronal circuits: back to the future. Neuron. 2012; 76(1):1–11. [PubMed: 23040802]

Martin JP, Beyerlein A, Dacks AM, Reisenman CE, Riffell JA, Lei H, Hildebrand JG. The neurobiology of insect olfaction: sensory processing in a comparative context. Prog Neurobiol. 2011; 95(3):427–447. [PubMed: 21963552]

Mercer AR, Hayashi JH, Hildebrand JG. Modulatory effects of 5-hydroxytryptamine on voltage-activated currents in cultured antennal lobe neurones of the sphinx moth Manduca sexta. J Exp Biol. 1995; 198(Pt 3):613–627. [PubMed: 7714451]

Mercer AR, Kloppenburg P, Hildebrand JG. Serotonin-induced changes in the excitability of cultured antennal-lobe neurons of the sphinx moth Manduca sexta. J Comp Physiol A. 1996; 178(1):21–31. [PubMed: 8568722]

Mustard JA, Beggs KT, Mercer AR. Molecular biology of the invertebrate dopamine receptors. Arch Insect Biochem Physiol. 2005; 59(3):103–117. [PubMed: 15986382]

Nusbaum MP, Blitz DM. Neuropeptide modulation of microcircuits. Curr Opin Neurobiol. 2012; 22(4):592–601. [PubMed: 22305485]

Nusbaum MP, Marder E. A modulatory proctolin-containing neuron (MPN). II. State-dependent modulation of rhythmic motor activity. J Neurosci. 1989; 9(5):1600–1607. [PubMed: 2566659]

Olsen SR, Wilson RI. Lateral presynaptic inhibition mediates gain control in an olfactory circuit. Nature. 2008; 452(7190):956–960. [PubMed: 18344978]

Pratt GE, Farnsworth DE, Fok KF, Siegel NR, McCormack AL, Shabanowitz J, Hunt DF, Feyereisen R. Identity of a second type of allatostatin from cockroach brains: an octadecapeptide amide with a tyrosine-rich address sequence. Proc Natl Acad Sci U S A. 1991; 88(6):2412–2416. [PubMed: 2006179]

Predel R, Rapus J, Eckert M. Myoinhibitory neuropeptides in the American cockroach. Peptides. 2001; 22(2):199–208. [PubMed: 11179813]

Reichwald K, Unnithan GC, Davis NT, Agricola H, Feyereisen R. Expression of the allatostatin gene in endocrine cells of the cockroach midgut. Proc Natl Acad Sci U S A. 1994; 91(25):11894–11898. [PubMed: 7991553]

Reisenman CE, Dacks AM, Hildebrand JG. Local interneuron diversity in the primary olfactory center of the moth Manduca sexta. J Comp Physiol A Neuroethol Sens Neural Behav Physiol. 2011; 197(6):653–665. [PubMed: 21286727]

Riffell JA, Lei H, Abrell L, Hildebrand JG. Neural basis of a pollinator's buffet: olfactory specialization and learning in Manduca sexta. Science. 2013; 339(6116):200–204. [PubMed: 23223454]

Root CM, Ko KI, Jafari A, Wang JW. Presynaptic facilitation by neuropeptide signaling mediates odor-driven food search. Cell. 2011; 145(1):133–144. [PubMed: 21458672]

Root CM, Masuyama K, Green DS, Enell LE, Nassel DR, Lee CH, Wang JW. A presynaptic gain control mechanism fine-tunes olfactory behavior. Neuron. 2008; 59(2):311–321. [PubMed: 18667158]

Rospars JP, Hildebrand JG. Sexually dimorphic and isomorphic glomeruli in the antennal lobes of the sphinx moth Manduca sexta. Chem Senses. 2000; 25(2):119–129. [PubMed: 10781018]

Roy B, Singh AP, Shetty C, Chaudhary V, North A, Landgraf M, Vijayraghavan K, Rodrigues V. Metamorphosis of an identified serotonergic neuron in the Drosophila olfactory system. Neural Dev. 2007; 2:20. [PubMed: 17958902]

Salecker I, Distler P. Serotonin-immunoreactive neurons in the antennal lobes of the American cockroach Periplaneta americana: light-and electron-microscopic observations. Histochemistry. 1990; 94(5):463–473. [PubMed: 2283309]

Salio C, Lossi L, Ferrini F, Merighi A. Neuropeptides as synaptic transmitters. Cell Tissue Res. 2006; 326(2):583–598. [PubMed: 16847638]

Saudou F, Boschert U, Amlaiky N, Plassat JL, Hen R. A family of Drosophila serotonin receptors with distinct intracellular signalling properties and expression patterns. EMBO J. 1992; 11(1):7–17. [PubMed: 1310937]

Siju KP, Reifenrath A, Scheiblich H, Neupert S, Predel R, Hansson BS, Schachtner J, Ignell R. Neuropeptides in the antennal lobe of the yellow fever mosquito, Aedes aegypti. J Comp Neurol. 2013

Singh AP, Das RN, Rao G, Aggarwal A, Diegelmann S, Evers JF, Karandikar H, Landgraf M, Rodrigues V, Vijayraghavan K. Sensory neuron-derived eph regulates glomerular arbors and modulatory function of a central serotonergic neuron. PLoS Genet. 2013; 9(4):e1003452. [PubMed: 23637622]

Su CY, Wang JW. Modulation of neural circuits: how stimulus context shapes innate behavior in Drosophila. Curr Opin Neurobiol. 2014; 29:9–16. [PubMed: 24801064]

Sun XJ, Tolbert LP, Hildebrand JG. Ramification pattern and ultrastructural characteristics of the serotonin-immunoreactive neuron in the antennal lobe of the moth Manduca sexta: a laser scanning confocal and electron microscopic study. J Comp Neurol. 1993; 338(1):5–16. [PubMed: 8300899]

Tripathy SJ, Peters OJ, Staudacher EM, Kalwar FR, Hatfield MN, Daly KC. Odors Pulsed at Wing Beat Frequencies are Tracked by Primary Olfactory Networks and Enhance Odor Detection. Front Cell Neurosci. 2010; 4:1. [PubMed: 20407584]

Utz S, Huetteroth W, Vomel M, Schachtner J. Mas-allatotropin in the developing antennal lobe of the sphinx moth Manduca sexta: distribution, time course, developmental regulation, and colocalization with other neuropeptides. Dev Neurobiol. 2008; 68(1):123–142. [PubMed: 17948246]

Utz S, Huetteroth W, Wegener C, Kahnt J, Predel R, Schachtner J. Direct peptide profiling of lateral cell groups of the antennal lobes of Manduca sexta reveals specific composition and changes in neuropeptide expression during development. Dev Neurobiol. 2007; 67(6):764–777. [PubMed: 17443823]

Utz S, Schachtner J. Development of A-type allatostatin immunoreactivity in antennal lobe neurons of the sphinx moth Manduca sexta. Cell Tissue Res. 2005; 320(1):149–162. [PubMed: 15726421]

Veenstra JA, Hagedorn HH. Isolation of two AKH-related peptides from cicadas. Arch Insect Biochem Physiol. 1995; 29(4):391–396. [PubMed: 7655059]

Wagh DA, Rasse TM, Asan E, Hofbauer A, Schwenkert I, Durrbeck H, Buchner S, Dabauvalle MC, Schmidt M, Qin G, Wichmann C, Kittel R, Sigrist SJ, Buchner E. Bruchpilot, a protein with homology to ELKS/CAST, is required for structural integrity and function of synaptic active zones in Drosophila. Neuron. 2006; 49(6):833–844. [PubMed: 16543132]

Waldrop B, Christensen TA, Hildebrand JG. GABA-mediated synaptic inhibition of projection neurons in the antennal lobes of the sphinx moth, Manduca sexta. J Comp Physiol A. 1987; 161(1):23–32. [PubMed: 3039128]

Wegerhoff R. GABA and serotonin immunoreactivity during postembryonic brain development in the beetle Tenebrio molitor. Microsc Res Tech. 1999; 45(3):154–164. [PubMed: 10344767]

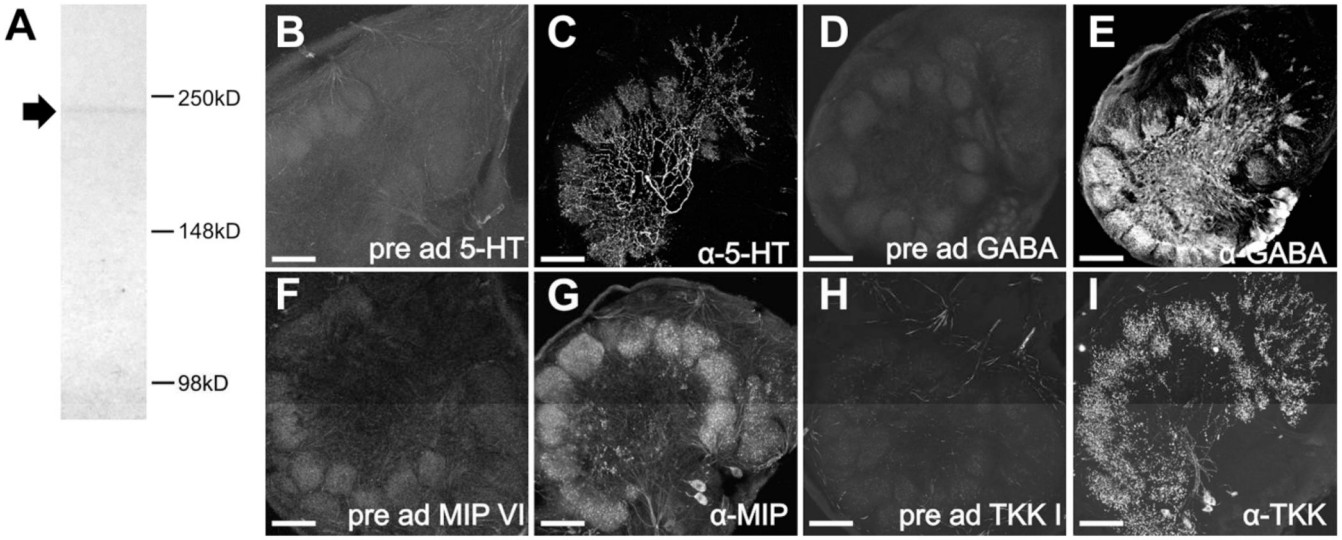

Figure 1.

Western blot of BRP antibody using *Manduca* brain tissue and pre-adsorption controls for the 5-HT, GABA, MIP and TKK antibodies. **A:** Western blots of *Manduca* brain tissue with the BRP antibody resulted in a single band at the predicted height for the *Manduca* homologue of the ELKS/CAST protein protein (~234kDa). The BRP antibody was used to mark glomerular outlines. **B:** Pre-adsorption of the goat anti-5-HT antiserum by incubating with 1mg/mL BSA and 10:1 5-HT-BSA conjugate:goat anti-5-HT antibody for 24hrs at 4°C abolished all staining of *Manduca* AL tissue. **C:** Non-pre-adsorbed controls in which goat anti-5-HT antibody was incubated in parallel under identical conditions with the exception of the 5-HT-BSA conjugate resulted in strong immunolabeling. **D:** Pre-adsorption of the rabbit anti-GABA antiserum by incubating with 1mg/mL BSA and 10:1 GABA:rabbit anti-GABA antibody for 24hrs at 4°C abolished all staining of *Manduca* AL tissue. **E:** Non-pre-adsorbed controls in which rabbit anti-GABA antibody was incubated in parallel under identical conditions with the exception of GABA resulted in strong immunolabeling. **F:** Pre-adsorption of the rabbit anti-MIP antiserum by incubating with 1mg/mL BSA and 10:1 synthetic MIP_{VI} (AWSALHGAWA): rabbit anti-MIP antibody for 24hrs at 4°C abolished all staining of *Manduca* AL tissue. **G:** Non-pre-adsorbed controls in which rabbit anti-MIP antibody was incubated in parallel under identical conditions with the exception of the synthetic MIP_{VI} resulted in strong immunolabeling. **H:** Pre-adsorption of the rabbit anti-TKK antiserum by incubating with 1mg/mL BSA and 10:1 synthetic TKK_I (RAPMGFMGVR): rabbit anti-TKK antibody for 24hrs at 4°C abolished all staining of *Manduca* AL tissue. **I:** Non-pre-adsorbed controls in which rabbit anti-TKK antibody was incubated in parallel under identical conditions with the exception of the synthetic TKK_I resulted in strong immunolabeling. Scale bar = 100 um.

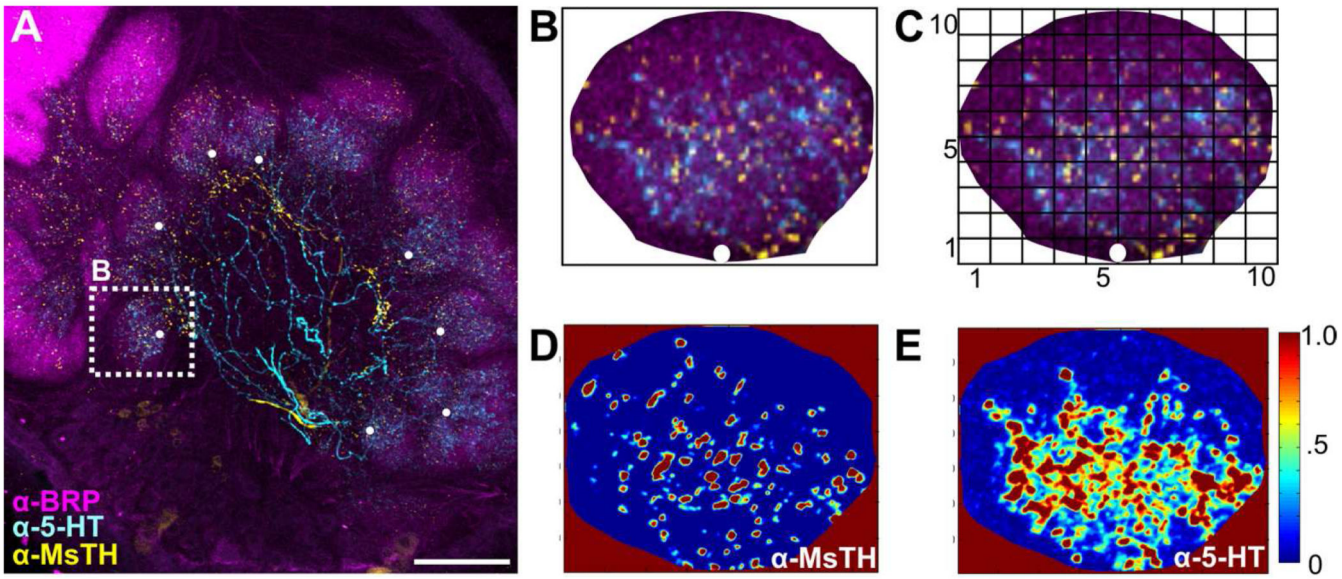

Figure 2.

Depiction of Intensity Distribution Analysis. **A:** Example .tif stack of an AL scan with glomeruli marked with a white dot at their most proximal, central point. **B:** Cropped glomerulus, marked in Fig. 2A, oriented such that the white dot is at the "6 o'clock" position to ensure that horizontal bin 1 always corresponds to the most proximal end of the glomerulus and horizontal bin 10 to the most distal. A white bordered square was placed with edges flush to the cropped glomerulus. The square is shown as black here to visualize concept. **C:** The area innervated and the density of pixels for each modulator was determined across a 10×10 matrix using a custom MatLAB script. Horizontal Bin 1 is most proximal, while horizontal bin 10 is most distal. **D:** MatLAB determined intensity values for MsTH-ir. **E:** MatLAB determined intensity values for 5-HT-ir. Scale bar = 100 um.

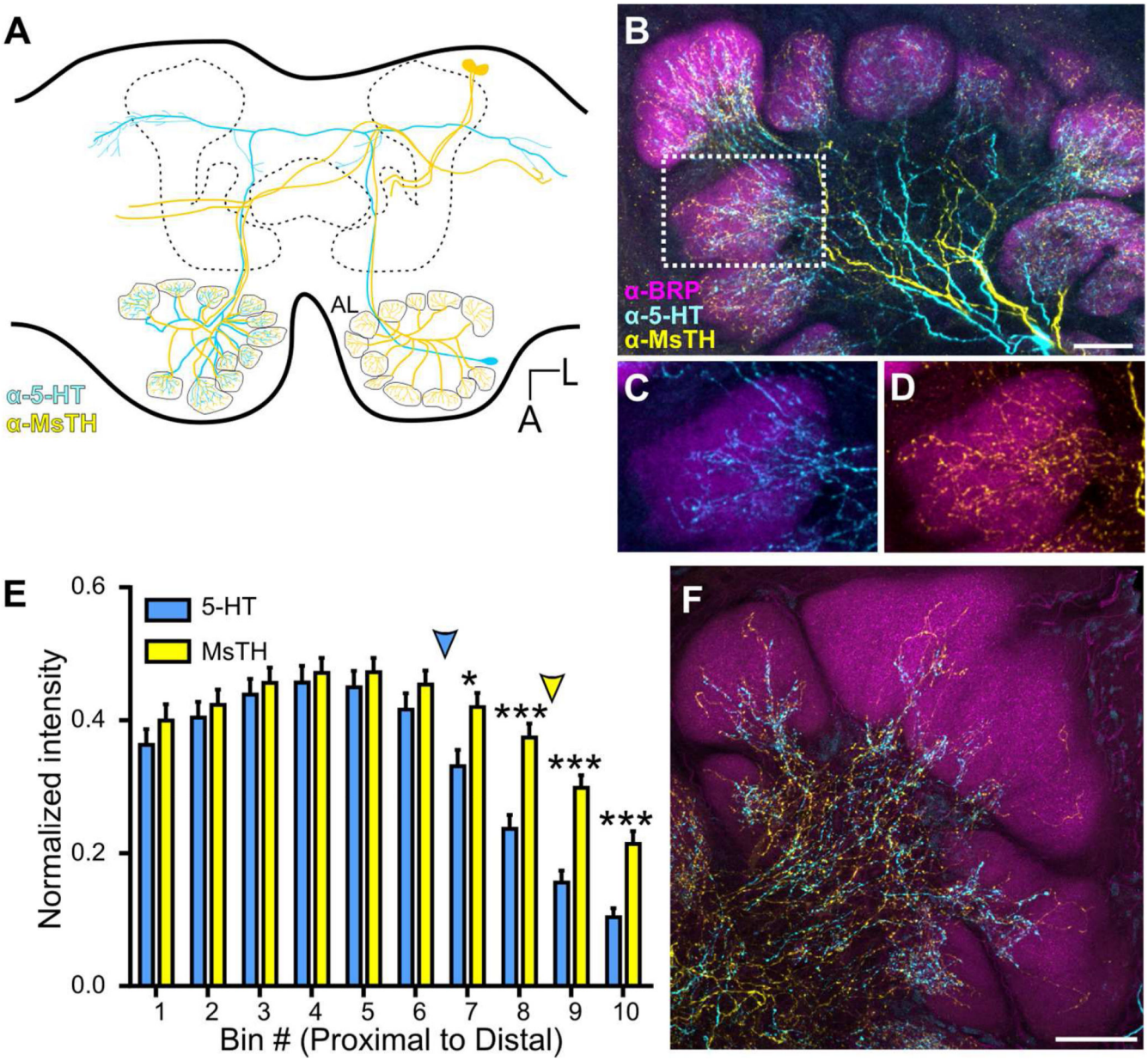

Figure 3.

Convergence of 5-HT-ir and MsTH-ir in AL glomeruli. **A:** Schematic of one pair of DAAR neurons (yellow) and a single CSD (blue) neuron within the brain of *Manduca*. The CSD cell bodies are located in the lateral cell cluster, while the DAAR cell bodies are located in the dorsal protocerebrum. Each AL is innervated by one CSD neuron which projects to the contralateral AL and innervates all glomeruli. Four DAAR neurons (one pair on each side of the brain) project to both the ipsilateral and contralateral ALs innervating all glomeruli. **B:** 5-HT-ir (cyan) is densely distributed near the proximal region of glomeruli while MsTH-ir (yellow) is distributed sparsely throughout glomeruli. Glomerular boundaries are delineated by BRP-ir (magenta). **C, D:** Inset from **B** depicting individual channels with 5HT-ir/BRP-ir and MsTH-ir/BRP-ir respectively. **E:** Glomerular distribution of 5-HT-ir and MsTH-ir along

the proximal to distal axis of isomorphic glomeruli. MsTH-ir extends farther distally than 5-HT (Multiple t-tests; t= 2.76 for bin7, t=4.55 for bin 8, t= 5.44 for bin 9, t= 4.68 for bin 10; df=18; p=0.012 for bin 7p<0.0001 for bin 8-10; n=100). The distribution of each modulator began to significantly reduce in intensity along the proximal to distal axis at different points. For 5-HT, intensity values began to significantly decrease at bin 6 (1-way ANOVA; p<0.01, df=9, n=10), while for MsTH, the intensity values don't begin to significantly decrease until bin 9 (1-way ANOVA; p<0.05, df=9, n=10). Colored arrowheads denote where the intensity of each modulator begins to significantly reduce. **F:** Macroglomerular complex (MGC) demonstrating sparse innervation of both 5-HT-ir and MsTH-ir. All scale bars = 50 um.

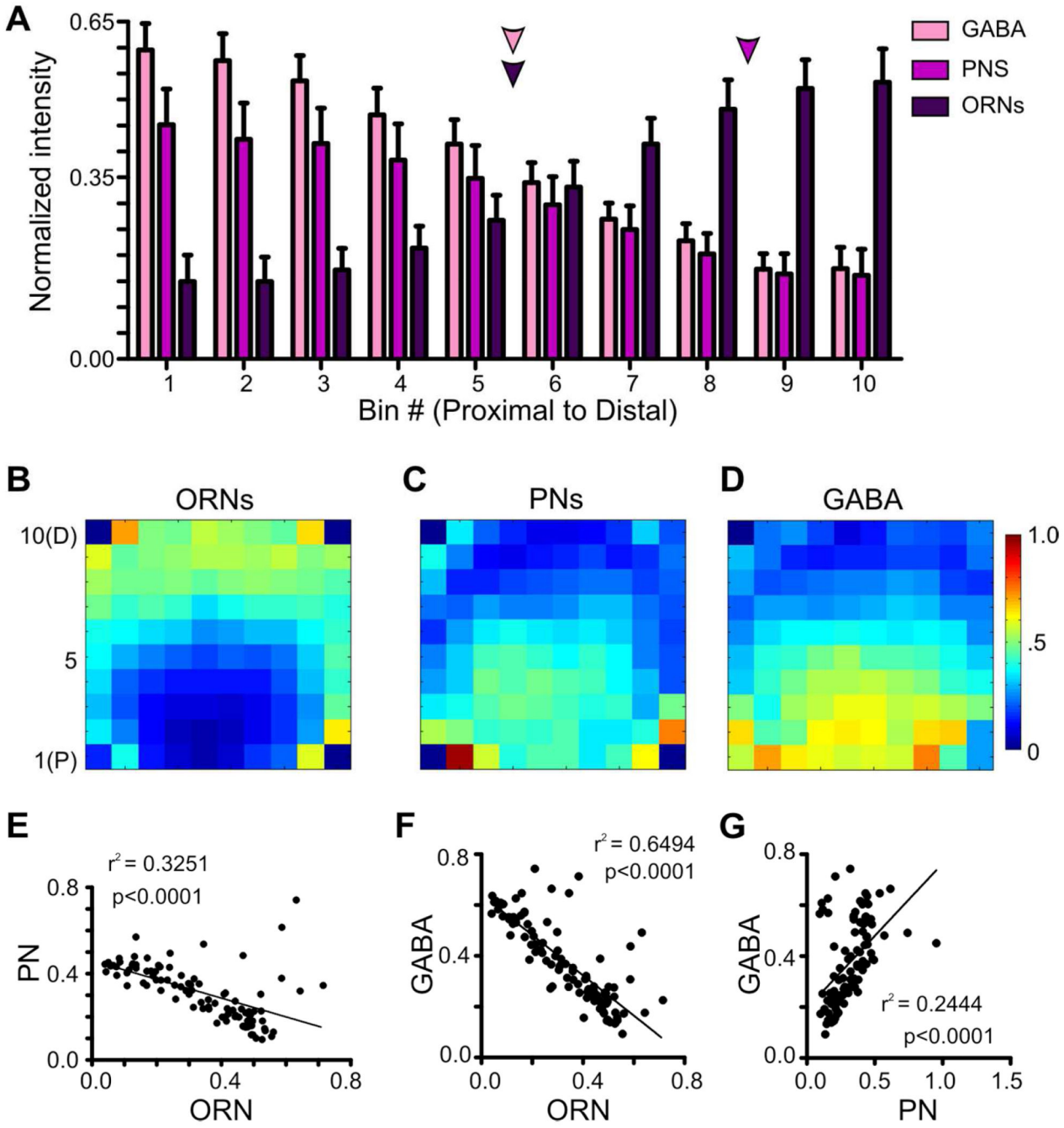

Figure 4.

The anatomical boundaries of ORNs, PNs and GABA-ir. **A:** Label intensity for ORNs,, PNs and GABA-ir along the proximal (bin 1) to distal (bin10) axis of a glomerulus. ORN intensity values began to significantly decrease relative to the most distal bin at bin 6 (1-way ANOVA; $p<0.05$, df=9, n=10). PNs intensity values began to significantly decrease relative to the most proximal bin at bin 9 (1-way ANOVA; $p<0.05$, d=9, n=10). GABA intensity values began to significantly decrease relative to the most proximal bin at bin 5 (1-way ANOVA; $p<0.01$, df=9, n=10). Colored arrows denote where the intensity of each neuronal

type begins to significantly reduce. **B-D:** Averaged 10×10 intensity plots for each neuron type (ORN, PN and GABA-ir, respectively. n=10 each). Blue denotes low intensity values, while red denotes high intensity values. **B:** 10×10 intensity plot for ORNs. **C:** 10×10 intensity plot for PNs. **D:** 10×10 intensity plot for GABA-ir. **E-G:** Linear regressions of the average intensities across the 10×10 intensity plots of ORNs, PNs and GABA-ir. **E:** The innervation patterns of ORNs and PNs display a negative relationship ($r^2 = 0.3251$, $p<0.0001$, n=10 glomeruli, 5 animals). **F:** ORNs and GABA display a negative relationship ($r^2 = 0.6494$, $p<0.0001$, n=10 glomeruli, 5 animals). **G:** The innervation patterns of PNs and GABA display a positive relationship ($r^2 = 0.2444$, $p<0.0001$, n=10 glomeruli, 5 animals).

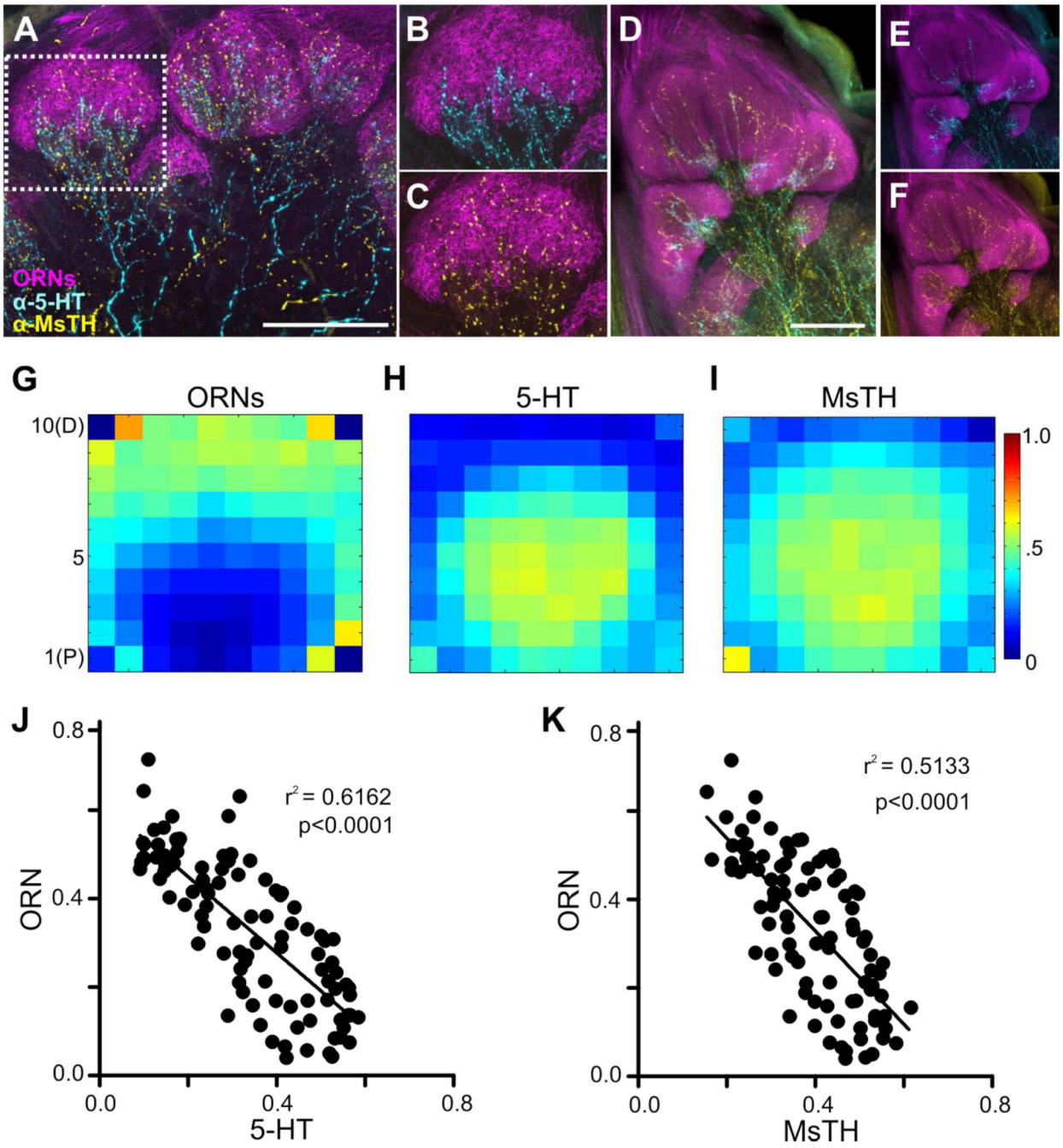

Figure 5.

Processes of the CSD and DAAR neurons innervate distinct glomerular zones with relation to ORNs. **A-C**: MsTH-ir (yellow) overlap with ORN axons (magenta) at the distal region of the glomerulus while 5-HT-ir (cyan) is constrained to proximal glomerular regions. **B**, **C**: Inset from **A** showing 5HT and MsTH branching, respectively, with relation to ORN axons in the glomerulus. **D-F**: MGC innervation by the CSD and DAAR neurons relative to ORN axons. All scale bars = 50 um. **G:** 10×10 intensity plot for ORNs. **H:** 10×10 intensity plot for 5-HT-ir. **I:** 10×10 intensity plot for MsTH-ir. **J-K:** Linear regressions of the average

intensities across the 10×10 intensity plots of ORNs, 5-HT-ir and MsTH-ir. **J:** 5-HT-ir and ORNs display a negative relationship ($r^2 = 0.6162$, $p<0.0001$). **K:** ORNs and MsTH-ir display a negative relationship ($r^2 = 0.5133$, $p<0.0001$).

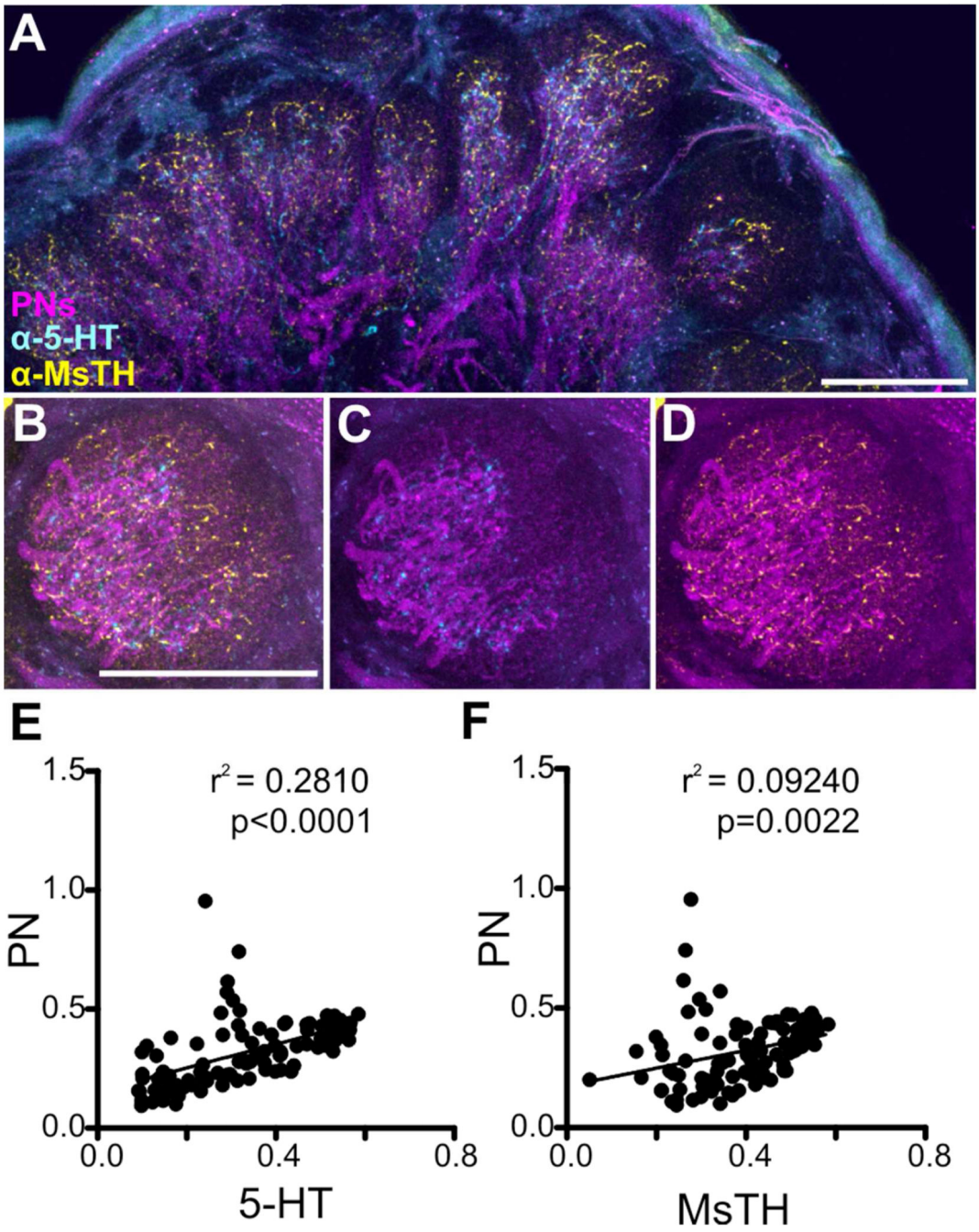

Figure 6.

CSD and DAAR neuron processes overlap extensively with the processes of PNs. **A**: The distribution of 5-HT-ir (cyan) and MsTH-ir (yellow) in isomorphic glomeruli relative to retrogradely filled PNs (magenta). **B-D**: High magnification examples of a glomerulus in which PNs, CSD and DAAR neurons have been labeled. **B:** PNs, 5-HT-ir and MsTH-ir depicted. **C**: PNs and 5-HT-ir depicted. **D**: PNs and MsTH-ir depicted. 5-HT-ir has nearly complete overlap with PNs, while MsTH-ir overlaps with PNs and extends distally. All scale bars = 50 um. **E-F:** Linear regressions of the average intensities across the 10×10 intensity

plots of PNs, 5-HT-ir and MsTH-ir. **E:** Linear regression 5-HT-ir and PNs display a positive relationship ($r^2 = 0.2810$, $p<0.0001$). **F:** PNs and MsTH-ir display a positive relationship ($r^2 = 0.09240$, $p = 0.0022$).

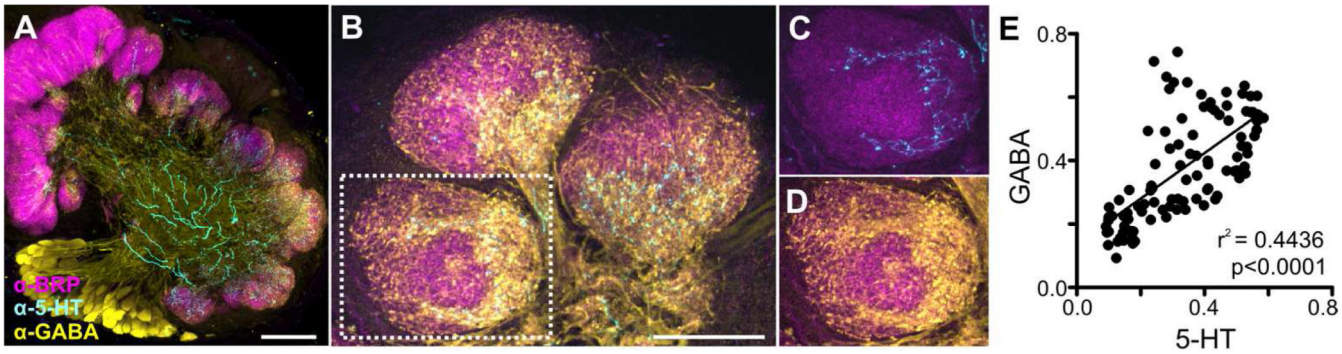

Figure 7.

CSD processes overlap extensively with processes of GABA-ir LNs and PNs **A:** AL immunolabeled for 5-HT (cyan), GABA (yellow) and BRP (magenta). Scale bar = 100 um. **B:** Distribution of 5-HT-ir and GABA-ir in isomorphic glomeruli. Scale bar = 50 um. **C-D:** Inset from **B** showing relative distribution of 5-HT-ir and GABA-ir within isomorphic glomeruli. **C:** 5-HT overlaps extensively with region occupied by the dense GABA-ir branching. **D:** GABA-ir extends throughout with denser processes at the proximal region and sparser innervation distally. **E:** Linear regression of the average intensities across the 10×10 intensity plots of 5-HT-ir and GABA-ir displaying a positive relationship (r^2 = 0.4436, $p<0.0001$).

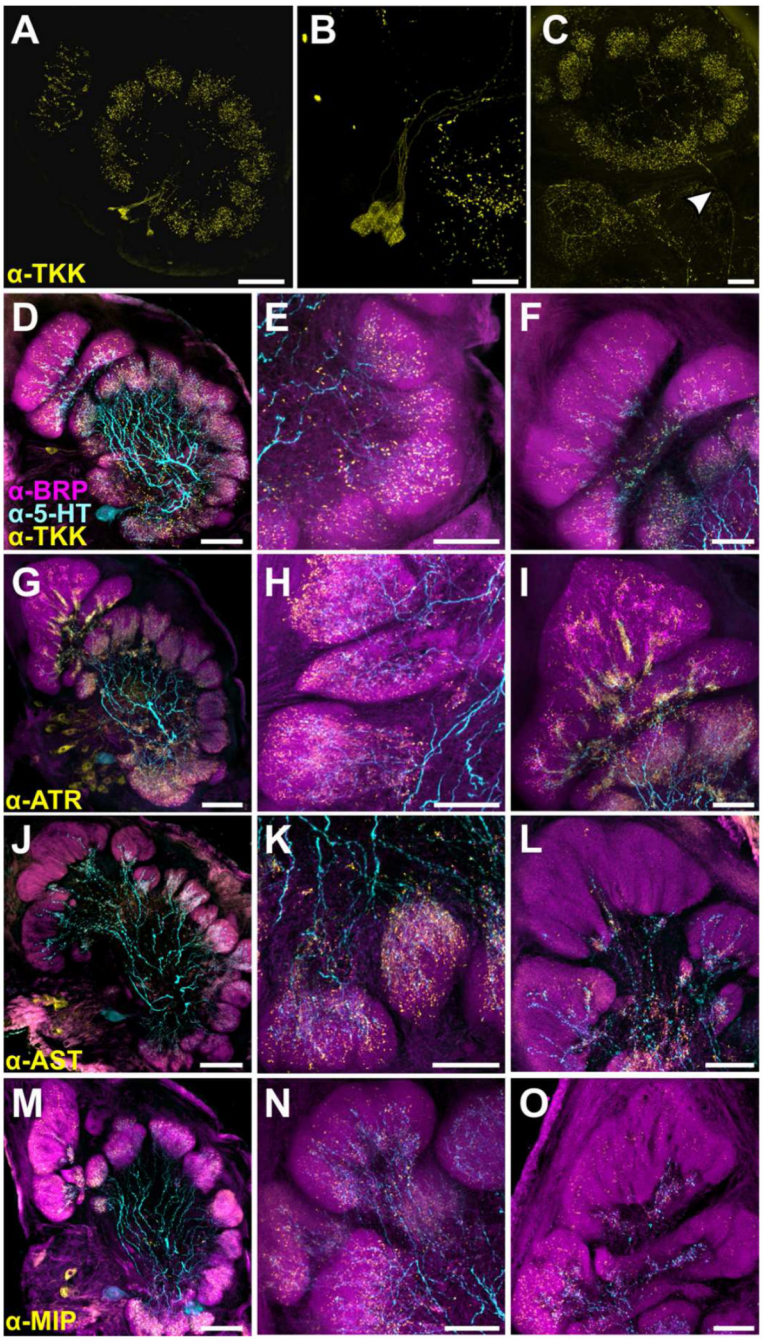

Figure 8.

Distribution of processes from peptidergic neurons and the CSD neurons. **A:** Tachykinin (TKK) labeling in the AL. Each AL features ~9 TKK-ir cell bodies which in sum innervate all glomeruli **B:** High resolution scan of TKK-ir cell bodies in the lateral cell cluster. **C:** TKK-ir process leaving the AL (denoted by white arrow). While most TKK-ir bodies appear to be LNs according to their morphology, the process leaves the AL via the mALT, suggesting that TKK-ir cells may be PNs or centrifugal neurons. **D-O:** Glomeruli stained for various neuropeptides (yellow), 5-HT (cyan) and BRP (magenta). Left column features the

AL (scale bars = 100 um), the middle column features a representative isomorphic glomerulus and the right column features a representative MGC (scale bars = 50 um). **D-E:** TKK-ir extends father distally than 5HT-ir in isomorphic glomeruli. **F:** TKK-ir extends farther distally in the MGC than 5-HT-ir. **G-I:** Dense processes of ATR-ir LNs occur in isomorphic glomeruli and extend farther distally than 5HT-ir. **I:** Allatotropin (ATR) processes in the MGC extend farther distally than 5-HT-ir. ATR-ir processes are dense proximally but more spare as they extend distally in the MGC. **J-L:** Allatostatin (AST) processes extend farther distally in the glomeruli than 5HT-ir and are uniform in density throughout. **L:** AST-ir sparsely innervates the MGC and remains proximal with 5-HT-ir. **M-O:** Myoinhibitory peptide (MIP) processes extend much farther distally than 5-HT-ir in the isomorphic glomeruli and are uniform in density throughout. **O:** MIP-ir extends farther distally than 5HT-ir within the MGC.

The antennal lobe (the first olfactory neuropil of the insect brain) of the moth Manduca sexta immunolabeled for serotonin (cyan) and GABA (yellow). Glomerular boundaries are highlighted with immunolabeling against bruchpilot (magenta).

Table 1

List of primary Antibodies

Antigen	Immunogen	Manufacturer, species antibody was raised in, monoclonal vs. polyclonal	Catalog #	RRID	Dilution used
5-HT	coupled to BSA w/ paraformaldehyde	Immunostar, goat, polyclonal	20079	AB_2313880	1:10,000
MsTH	Full MsTH protein sequence	Maureen Gorman, rabbit	N/A	N/A	1:5,000
γ-aminobutyric acid (GABA)	BSA w/ paraformaldehyde	Sigma-Aldrich, rabbit, polyclonal	A2052	N/A	1:500
BRP	Head homogenate	DSHB, mouse, monoclonal	Bruchpilot	AB_2314866	1:50
MIP	Coupled to thyroglobulin	Christian Wegener, rabbit, polyclonal	N/A	AB_2314803	1:3,000
ATR	Coupled to thyroglobulin w/ glutaraldehyde	Jan Veenstra, rabbit	N/A	AB_2313973	1:3,000
AST	Bovine thyroglobulin peptide-bovine serum albumin (BSA) conjugate in 0.05 ml of 0.1 M sodium bicarbonate	Jan Veenstra, rabbit, polyclonal	N/A	N/A	1:3,000
TKK	Bovine thyroglobulin with glutaraldehyde	Jan Veenstra, rabbit, polyconal	ABD-045	AB_2341129	1:4,000

Table 2

Abbreviations

5-HT	serotonin
AL	antennal lobe
AST	allatostatin
ATR	allatotropin
BRP	bruchpilot
CSD	contralaterally projecting serotonin immunoreactive deutocerebral neuron
DA	dopamine
DAAR	dopaminergic arching neuron
LNs	local interneurons
mALT	medial antennal lobe tract
MsTH	*Manduca sexta* tyrosine hydroxylase
ORNs	olfactory receptor neurons
PNs	projection neurons
SIFamide	AYRKPPFNGSIFamide
TH-ir	tyrosine hydroxylase immunoreactive
TKK	tachykinin